A novel mouse model of cerebral cavernous malformations based on the two-hit mutation hypothesis recapitulates the human disease

David A. McDonald[1], Robert Shenkar[2,‡], Changbin Shi[2,‡], Rebecca A. Stockton[3], Amy L. Akers[1,†], Melanie H. Kucherlapati[4], Raju Kucherlapati[4], James Brainer[5], Mark H. Ginsberg[3], Issam A. Awad[2,*,‡] and Douglas A. Marchuk[1,*,‡]

[1]Molecular Genetics and Microbiology Department, Duke University Medical Center, Durham, NC 27710, USA, [2]Section of Neurosurgery, Biological Sciences Division, University of Chicago, Chicago, IL 60637, USA, [3]Department of Medicine, University of California, San Diego, La Jolla, CA 92903, USA, [4]Department of Medicine, Brigham and Women's Hospital, Boston, MA 02115, USA and [5]Department of Pathology, University of Chicago Medical Center, Chicago, IL 60637, USA

Cerebral cavernous malformations (CCMs) are vascular lesions of the central nervous system appearing as multicavernous, blood-filled capillaries, leading to headache, seizure and hemorrhagic stroke. CCM occurs either sporadically or as an autosomal dominant disorder caused by germline mutation of one of the three genes: *CCM1/KRIT1*, *CCM2/MGC4607* and *CCM3/PDCD10*. Surgically resected human CCM lesions have provided molecular and immunohistochemical evidence for a two-hit (germline plus somatic) mutation mechanism. In contrast to the equivalent human genotype, mice heterozygous for a *Ccm1*- or *Ccm2*-null allele do not develop CCM lesions. Based on the two-hit hypothesis, we attempted to improve the penetrance of the model by crossing *Ccm1* and *Ccm2* heterozygotes into a mismatch repair-deficient $Msh2^{-/-}$ background. $Ccm1^{+/-} Msh2^{-/-}$ mice exhibit CCM lesions with high penetrance as shown by magnetic resonance imaging and histology. Significantly, the CCM lesions range in size from early-stage, isolated caverns to large, multicavernous lesions. A subset of endothelial cells within the CCM lesions revealed somatic loss of CCM protein staining, supporting the two-hit mutation mechanism. The late-stage CCM lesions displayed many of the characteristics of human CCM lesions, including hemosiderin deposits, immune cell infiltration, increased endothelial cell proliferation and increased Rho-kinase activity. Some of these characteristics were also seen, but to a lesser extent, in early-stage lesions. Tight junctions were maintained between CCM lesion endothelial cells, but gaps were evident between endothelial cells and basement membrane was defective. In contrast, the $Ccm2^{+/-} Msh2^{-/-}$ mice lacked cerebrovascular lesions. The CCM1 mouse model provides an *in vivo* tool to investigate CCM pathogenesis and new therapies.

INTRODUCTION

Cerebral cavernous malformations (CCMs) are vascular lesions of the central nervous system that consists of clusters of grossly dilated, brittle capillaries which proliferate in the setting of repetitive hemorrhage into large, multicavernous structures. It is estimated that more than 0.5% of the population harbor one or more such lesions, predisposing patients to a lifetime risk of hemorrhagic stroke, seizures and other clinical sequelae (1,2). Cases of CCM occur either

---

*To whom correspondence should be addressed at: Box 3175, Duke University Medical Center, Durham, NC 27710, USA. Tel: +1 9196841945; Fax: +1 9196842790; Email: march004@mc.duke.edu (D.A.M.); Section of Neurosurgery, 5841 S. Maryland Avenue, Room J338, M/C 3026, Chicago, IL 60637, USA. Tel: +1 7737022123; Fax: +1 7737023518; Email: iawad@uchicago.edu (I.A.A.)
†Present address: Angioma Alliance, Norfolk, VA 23517, USA.
‡Denotes equal contributions.

sporadically or in familial clusters in which the disease shows an autosomal dominant inheritance pattern. Mutations in three genes have been shown to cause CCM: *CCM1*/KRIT1 (3,4), *CCM2*/malcavernin (5,6) and *CCM3*/PDCD10 (7). Though their exact function is uncertain, the CCM proteins have been found to physically interact (8–10). Moreover, recent work shows that CCM1 is involved in actin reorganization through association with Rap1 (11) and inhibition of RhoA and Rho kinase (ROCK) (12–15).

Current understanding of the CCM vascular phenotype is based largely on the pathologic study of surgically resected lesions. The multicavernous structures are lined by a single layer of endothelium and are separated by a loose, collagenous matrix lacking mature vessel wall structure. The endothelial layer lining the caverns manifests gross breaches, including vacuoles and apparently defective inter-endothelial cell junctions, and seems to lack well-developed basement membrane and other structural integrity of blood-brain barrier (16–18). The disruption of the blood-brain barrier and brittle structure of the vascular wall are thought to account for repetitive hemorrhages and reactive changes in adjacent brain. Gene expression arrays have revealed a number of genes with altered expression in human CCM tissue. Increased expression of nine immunoglobulin genes (19) implicates a role of immune response in the pathology of the disease. This is further validated by evidence of an oligoclonal IgG immune response in human CCM tissue (20,21), which suggests that the immune system is responding to a specific antigen in the lesion that is not present in normal cerebral blood vessels.

Sporadic cases of CCM are characterized by an isolated lesion, whereas familial cases usually exhibit multiple lesions in random distribution throughout the brain with increasing prevalence of lesions during patients' lifetime (22,23). Based on these observations, we and others hypothesized that CCM lesion genesis follows a two-hit mutation mechanism, where both copies of a gene must be inactivated in the same cell to initiate lesion genesis. In familial cases, a germline mutation is inherited in one allele and lesions would arise from somatic mutations of the wild-type allele. There is growing evidence for a two-hit mechanism in human CCM lesion samples as multiple studies have identified somatic mutations in surgically resected human lesions (24–26). Most of these somatic mutations are single-base changes or small insertions/deletions that would be predicted to inactivate the protein. Another study found a loss of CCM protein immunostaining in the lesional vascular endothelium corresponding to the gene harboring the germline mutation, providing additional, biochemical evidence of a somatic mutational event (27).

Despite the knowledge gained thus far, analysis of mature, late-stage CCM lesions may not reflect the earliest pathologic changes associated with lesion genesis. Magnetic resonance imaging (MRI) data can show the appearance of new lesions and growth of existing lesions over time (22). Although the earliest stages of lesion development have been increasingly described with advanced MRI techniques (23,28), they are neither manifested clinically nor are they readily available for pathologic examination. A major gap is the ability to study lesion genesis and progression *in vivo*.

To address these questions, we have created mouse models of CCM. The development of the *Ccm1* knockout allele has been described previously (29), as has the gene-trap insertion used to generate the *Ccm2* knockout allele (30). Mice homozygous for the knockout alleles of either *Ccm1* or *Ccm2* die mid-gestation and heterozygous animals do not show lesions at an appreciable frequency (12,29,30). Based on the two-hit mechanism, we hypothesized that lesion penetrance of the heterozygous CCM mice could be increased by crossing the mutation into a genetic background with elevated genetic instability. Homozygous knockout of *Trp53*, a tumor suppressor gene, increases the overall rate of somatic mutations. We employed this mutant allele as a genetic sensitizer to attempt to increase the penetrance of the CCM mutant alleles. Mice that are heterozygous for either *Ccm1* or *Ccm2* in the presence of a homozygous knockout of *Trp53* show an increase in cerebral CCM lesions compared with control mice with a penetrance of approximately 30% (31,32). Lesions can be seen both externally and in coronal cross-sections. By both MRI and histology, these mouse lesions closely resemble CCM lesions surgically removed from humans.

Homozygous knockout of *Trp53* creates a background of increased genomic instability (33), most often gross chromosomal abnormalities and large insertions/deletions. In light of the broad genomic effects and systemic sequelae of the *Trp53*-null background (34), this model is not well suited for therapeutic testing. We sought to create a next-generation model that would initiate lesion genesis by generating somatic mutations more closely resembling those seen in surgically resected, mature CCM lesions from patients, and with lesser genomic sequelae and systemic side effects. Homozygous knockout of *Msh2*, a component of the mismatch repair complex, increases the overall rate of somatic point mutations and 1–3 bp insertions/deletions (35). The *Msh2*-null background was first used to sensitize $Apc^{+/-}$ mice to generate a more robust and penetrant intestinal neoplasia phenotype (36). Owing to their more penetrant phenotype, the compound mutant $Apc^{+/-}Msh2^{-/-}$ mice have been used for studies of therapeutic interventions (37,38). In a similar fashion, we used the *Msh2*-null genotype as a new genetic sensitizer to increase the probability of somatic mutation and, thereby, lesion burden of the Ccm heterozygous mice. In the present study, we show that this new mouse model can develop CCM lesions with relevant phenotypic features of human lesions, and that it allows us to capture CCM lesions at multiple stages of development, including what appear to be the early precursors of the mature CCM lesion.

RESULTS

An *Msh2* knockout allele was generated by crossing mice with an allele of *Msh2* flanked by loxP sites (39) with a strain of mice bearing the Cre recombinase transgene under control of the ubiquitous promoter EIIa (The Jackson Laboratory, stock number 003724). After a stably transmitting *Msh2*-null allele was generated, the Cre recombinase was bred out of the mice to prevent unforeseen effects of the transgene. The resulting $Msh2^{+/-}$ animals were then crossed with $Ccm1^{+/-}$
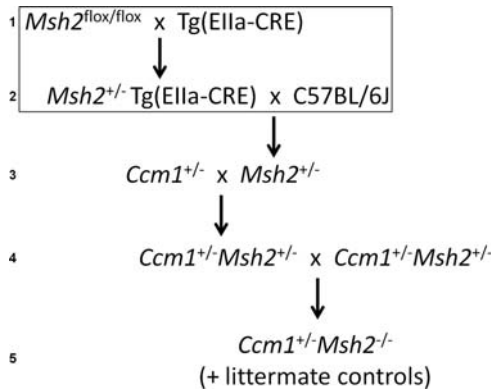
Figure 1. Breeding scheme to create $Ccm1^{+/-}Msh2^{-/-}$ mice. A two-generation cross was used to produce the *Msh2* knockout allele (box). The first cross generated the *Msh2* knockout allele using CRE-lox technology and the second cross aimed at breeding out the CRE transgene by back-crossing mice to C57BL/6J. From that point, a three-generation cross produces $Ccm1^{+/-}Msh2^{-/-}$ mice. First, *Msh2* heterozygotes without the CRE transgene were crossed with mice heterozygous for *Ccm1*. Double heterozygotes from this cross were mated with each other in the fourth generation to produce $Ccm1^{+/-}Msh2^{-/-}$ mice as well as littermate controls. A similar breeding scheme was used to generate $Ccm2^{+/-}Msh2^{-/-}$ mice.

or $Ccm2^{+/-}$ mice (29,30) to produce the double heterozygotes $Ccm1^{+/-}Msh2^{+/-}$ and $Ccm2^{+/-}Msh2^{+/-}$. These mice were separately intercrossed to generate $Ccm1^{+/-}Msh2^{-/-}$ and $Ccm2^{+/-}Msh2^{-/-}$ offspring as well as the littermate controls used in this study: $Ccm1^{+/-}Msh2^{+/-}$, $Ccm1^{+/+}Msh2^{-/-}$, $Ccm2^{+/-}Msh2^{+/-}$ and $Ccm2^{+/+}Msh2^{-/-}$. A summary of the crosses used to generate $Ccm1^{+/-}Msh2^{-/-}$ mice is shown in Fig. 1 and a similar schematic was used for $Ccm2^{+/-}Msh2^{-/-}$ mice. Importantly, all mouse lines have been maintained by back-crossing with C57BL/6J mice for at least 12 generations to avoid unwanted phenotype effects from different strain backgrounds. Random mice from each line were selected for single-nucleotide polymorphism (SNP) genotyping (Illumina GoldenGate 377 mouse SNP panel) to ensure that the genetic background of the mice was pure. SNP genotyping showed that the genomes of the mice were uniformly derived from C57BL/6J except for the regions surrounding the knockout alleles, which were originally derived from 129X1Sv/J (for *Ccm1*), 129P2/OlaHsd (for *Ccm2*) or WW6 (for *Msh2*) backgrounds (data not shown).

$Ccm1^{+/-}$ and $Ccm2^{+/-}$ mice have repeatedly shown extremely low, and in most cases no, penetrance of CCM lesions (29–32). To test the hypothesis that lesion formation is a stochastic, time-dependent process, which might occur over longer timespans, we aged three animals of each genotype between 1 and 3 years before sacrifice. Even under these conditions, no lesions were identified by high-field *ex vivo* MRI (data not shown). Thus, it was necessary to sensitize the heterozygous animals in order to uncover the CCM phenotype.

Homozygous knockout of *Msh2* will create a genetic background of somatic mismatch repair deficiency and, thus, an increased probability of somatic mutation of the wild-type allele of *Ccm1* or *Ccm2*. However, $Msh2^{-/-}$ mice are prone to lymphoma and small intestinal tumors by 6 months of age (39–41), so to avoid cancer-induced morbidity and mortality in this CCM model, we sacrificed the animals at 4–5

Table 1. Penetrance of CCM lesions in the mouse models

Genotype	Total no. of mice	Fraction of mice with CCM lesions
$Ccm1^{+/-}$	3	0/3
$Ccm2^{+/-}$	3	0/3
$Msh2^{-/-}$	6	0/6
$Ccm1^{+/-}Msh2^{-/-}$	19	9/19
$Ccm2^{+/-}Msh2^{-/-}$	11	0/11

months of age (4.4 ± 0.5 months for $Ccm1^{+/-}Msh2^{-/-}$, 5.1 ± 1.5 months for $Ccm2^{+/-}Msh2^{-/-}$). At sacrifice, brains were removed, fixed by immersion and screened for CCM lesions using gradient echo *ex vivo* high-field MRI. Subsequently, 2 mm serial coronal sections of the brains were surveyed histologically by hematoxylin and eosin (H&E) staining (32). Although *Msh2*-null mice have not been reported to develop cerebral vascular disease, we examined six $Msh2^{-/-}$ mouse brains by MRI and found neither tumors nor CCMs (Table 1). However, when knockout of *Msh2* was used as a sensitizer in *Ccm1* heterozygous mice, CCM lesions were observed by *ex vivo* MRI and histology.

In the sensitized mice, lesions were found at varying stages of development, from smaller, early-stage, isolated caverns to late-stage, multicavernous lesions. To differentiate between these stages, we defined stage 1 CCM lesions as dilated capillaries having the width at least 25 red blood cells and not joined to any other lesion (isolated caverns) and stage 2 lesions as multicavernous structures composed of the confluence of two or more caverns (32). Using these definitions, 9 out of the 19 (47.3%) $Ccm1^{+/-}Msh2^{-/-}$ animals exhibited one or more lesions compared with none of the 6 $Msh2^{-/-}$ mice examined ($P = 0.007$, two-tailed Fisher's exact test). Seven $Ccm1^{+/-}Msh2^{-/-}$ mice had only isolated, stage 1 lesions, five had complex, multicavernous stage 2 lesions and three animals harbored both stage 1 and stage 2 lesions. By contrast, none of the 11 $Ccm2^{+/-}Msh2^{-/-}$ mice exhibited any such lesions. H&E staining with stereotactic localization of the MRI lesion confirmed CCM histology in each case (Fig. 2), and no occult lesions were found on contiguous serial coronal sections (separated by 2 mm) of seven brains lacking suspected lesions by *ex vivo* MRI.

With systemic screening by MRI and histopathology, lymphoma was found in only one $Ccm2^{+/-}Msh2^{-/-}$ mouse. Lymphoma was confirmed by strong homogenous CD45 (leukocyte common antigen) immunostaining. Systemic examination of 38 additional $Msh2^{-/-}$ animals revealed no brain tumors by MRI or histology. This brain tumor prevalence of approximately 2.6% compares to a greater than 11.1% prevalence we had observed in the $Trp53^{-/-}$ animals (32). Animal attrition in this model, representing an index of systemic disease, was 10.3% until age 5 months in $Msh2^{-/-}$ mutants compared with 48% in those with $Trp53^{-/-}$ background. Thus, compared with the previous model (31,32), this new model shows lower morbidity and mortality.

Phenotypic maturation of CCM lesions

The ability to visualize CCM lesions on MRI in humans depends on the accumulation of hemosiderin deposits around
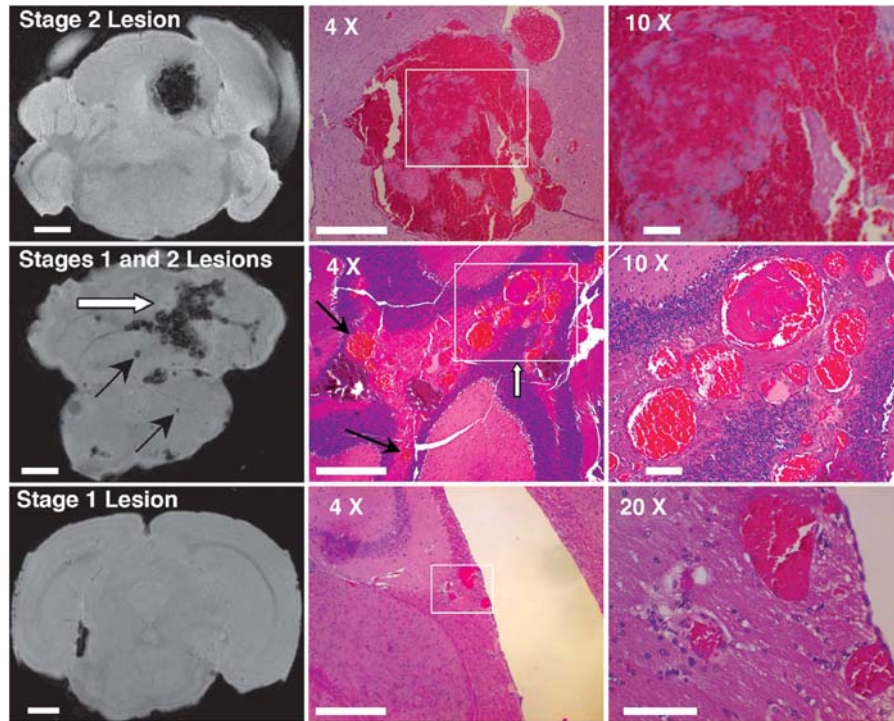
Figure 2. Characterization of lesions in $Ccm1^{+/-}Msh2^{-/-}$ mice. Both stage 1 (isolated dilated vessels) and stage 2 (clusters of dilated vessels) are found in the brains of the mice. Images are shown of coronal sections of brains from gradient recalled echo magnetic resonance (left) and H&E staining. The boxes in the middle panels denote the area represented under higher magnification in the right panels. In the middle row, black arrows denote representative stage 1 lesions and white arrows denote a stage 2 lesion. Scale bars are 1 mm (left), 0.5 mm (center) and 0.1 mm (right).

the lesion. Iron deposits around the mouse CCM lesions, identified by Perls' staining, were found in four of the five stage 2 lesions (Fig. 3), and the intensity of iron deposits showed remarkable variation (from a few iron particles per lesion to a high density of iron surrounding the lesion). By contrast, there was no iron deposition in any of the approximately 40 stage 1 lesions examined ($P = 0.048$, two-tailed Fisher's exact test). Thus, this mouse model of CCM provides a means of studying late-stage lesions that behave similarly to those seen in the multicavernous human lesion samples. Additionally, the model allows the study of CCM lesions at an earlier stage of development before hemosiderin deposits form.

Gene expression data from surgically resected human CCM lesions suggest a role for the immune response in CCM pathology (19). Furthermore, the prevalence of immune cells surrounding CCM lesions has been studied and an immune response may occur against an antigen specific to CCM lesions (20,21). As in late-stage human lesions, infiltration of immunocompetent cells, including B cells, plasma cells and macrophages, was observed in three of the three $Ccm1^{+/-}Msh2^{-/-}$ stage 2 lesions examined (Fig. 3). However, only a small subset of stage 1 mouse lesions showed evidence of immune cell infiltration. The number of cells per total caverns counted for stage 1 versus stage 2 lesions was, respectively, 0.61 versus 3.1 for B lymphocytes, 0.52 versus 1.5 for plasma cells and 0.05 versus 0.2 for macrophages. There was a trend for significance in differences in the B-cell density between stage 1 and stage 2 lesions ($P = 0.06$ by the Wilcoxin two-sample test). Based on these results,

this mouse model recapitulates what is seen for the immune response in late-stage, resected human CCM lesions. Using this murine model, we are now able to examine early-stage lesions for how the presence of immune cells may determine the natural history of lesion progression.

Increased cell proliferation has been proposed as a mechanism for the growth of CCM lesions, and previous studies examining this process in late-stage human CCM lesion tissue have found evidence of proliferating endothelial cells (42,43). The stage of CCM development when proliferation occurs is unknown. Expression of Ki-67, a proliferation-associated nuclear protein, around mouse CCM lesions was present in the endothelial cells within stage 2 lesions, but not in stage 1 lesions (Fig. 3). When comparing stage 1 versus stage 2 lesions, respectively, there were 0 versus 50% caverns with Ki-67 positive endothelial cells per total caverns counted ($P < 0.001$, Fisher's exact test) and 0 versus 11% Ki-67 positive endothelial cells per total number of endothelial cells counted ($P < 0.001$, Fisher's exact test). From these data, cell proliferation appears to only be important in larger multicavernous CCM lesions, but not at the earliest stages of grossly dilated isolated caverns. Using this mouse model of CCM, we can determine when endothelial cells become proliferative during lesion progression and how this affects lesion development.

ROCK activation in background vessels and CCM lesions

Recent studies in human endothelial cell culture have found that CCM2 regulates RhoA activity, which may regulate
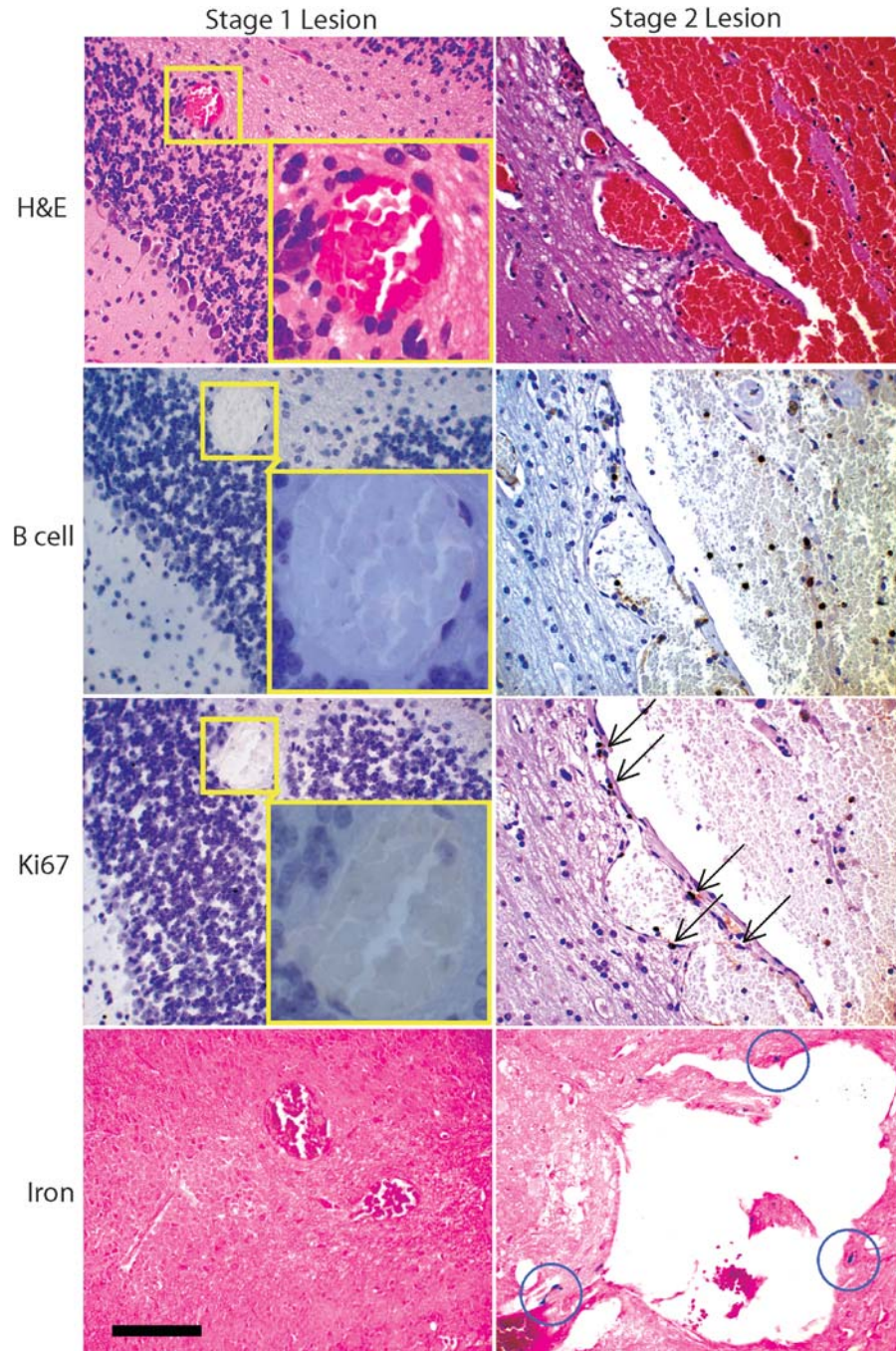
Figure 3. Phenotypic maturation in stage 1 versus stage 2 lesions. Stage 2 lesions (right panels) in brains from $Ccm1^{+/-}Msh2^{-/-}$ mice harbor B cells (brown B220), proliferating endothelium (brown Ki67) and iron (blue Perl stain). These are not visible in stage 1 lesions (left panels). Images are shown at ×3 higher magnification in the respective insets. Circles indicate blue iron particles in stage 2 multicavernous lesions (bottom right panel). Scale bar is 100 μm.

endothelial cell migration, lumen formation and vascular permeability (12). Furthermore, knockdown of *CCM1* or *CCM2* genes increases RhoA activity (12–14). ROCK, a downstream effector of RHOA, shows increased activity in late-stage human CCM lesion tissue (14) and mouse endothelial cell culture (13,15). We measured ROCK activity by phosphorylation of myosin light chain (pMLC) within the endothelial cells (13–15) of stage 1 and stage 2 lesions from $Ccm1^{+/-}Msh2^{-/-}$ mice as well as $Msh2^{-/-}$ control mouse

brain specimens (Fig. 4). We quantified the relative pMLC staining intensity of the lesions in order to analyze the data for statistical significance. Each vessel or lesion was assessed for staining independently by two investigators using the following categories: 'none' (completely absent of pMLC staining), 'weak' (definite, but diffuse staining) and 'strong' (intense and confluent staining). Using a scale (0/1/2 for none/weak/strong), the intensity of pMLC staining increased significantly with the size and complexity of the vessels/
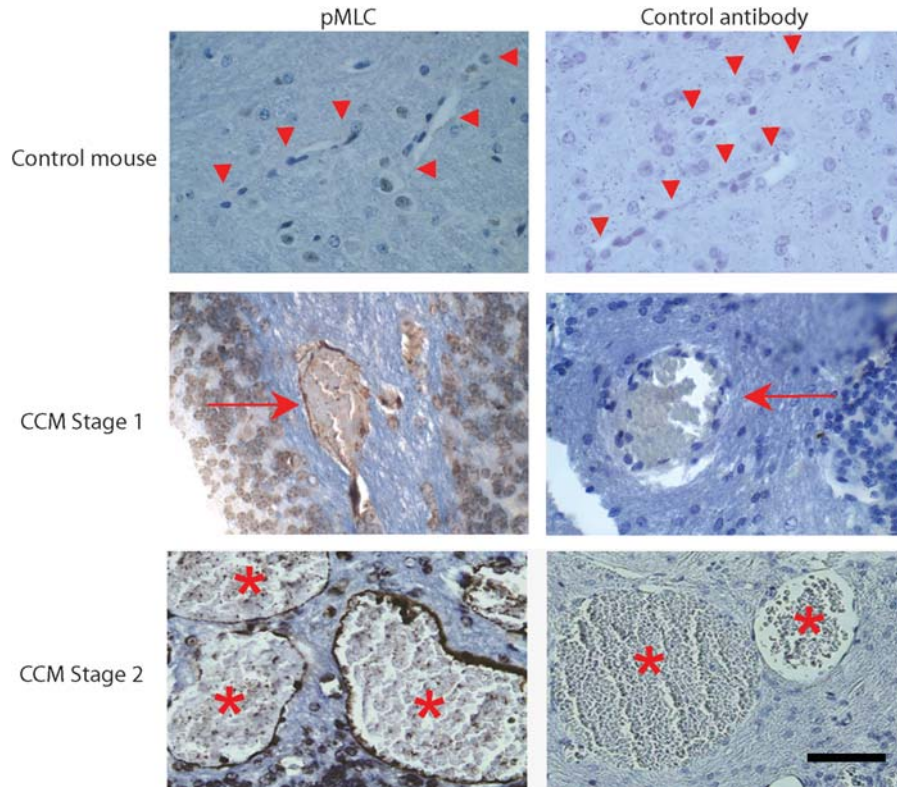
Figure 4. ROCK activation in mouse CCM lesions. ROCK activation was assessed by pMLC immunohistochemistry (dark brown staining, left panels). Normal capillaries (arrowheads) from an $Msh2^{-/-}$ control mouse (top row) do not show evidence of ROCK activation. By contrast, in $Ccm1^{+/-}Msh2^{-/-}$ mice, endo-thelial cells (ECs) lining stage 1 lesions (arrows) stain weakly for pMLC (middle row) and ECs lining three caverns (asterisks) of a stage 2 lesion show stronger pMLC staining. Corresponding serial sections show no staining with an isotype control (right panels). All tissue sections were counterstained blue with hema-toxylin. Scale bar is 100 μm.

lesions (capillaries < stage 1 < stage 2) in brains with CCM lesions (Fig. 5A). Normal capillaries in brains from $Ccm1^{+/-}Msh2^{-/-}$ mice with CCM lesions had significantly stronger pMLC staining than those from mice with the same genotype without CCM lesions, and these in turn had stronger pMLC staining than those from $Msh2^{-/-}$ control mice (Fig. 5B). From this, it is apparent that this mouse model not only validates the previous findings in late-stage human CCM lesions and cell culture, but it also provides a means of staging ROCK activity in background normal capillaries and in CCM lesions during disease progression.

Loss of KRIT1 protein in lesions from $Ccm1^{+/-}Msh2^{-/-}$ mice

In support of a two-hit mechanism in CCM, two groups have independently shown a loss of particular CCM protein expression in the endothelial cells surrounding human CCM caverns (14,27). We sought to confirm these results in the mouse model to show that it faithfully recapitulates the human disease. Coronal sections from brains removed from one $Msh2^{-/-}$ control, one $Ccm2^{+/-}Msh2^{-/-}$ and four $Ccm1^{+/-}Msh2^{-/-}$ mice were stained with anti-KRIT1 and anti-CCM2 primary antibodies for analysis by immunohisto-chemistry (Fig. 6). Capillary endothelial cells in $Msh2^{-/-}$ control brains showed robust expression of KRIT1 and CCM2. Normal capillaries in $Ccm2^{+/-}Msh2^{-/-}$ brain also

showed robust KRIT1 endothelial cell expression, but reduced expression of CCM2 (data not shown), as expected in animals heterozygous for *Ccm2*. Normal capillaries in four $Ccm1^{+/-}Msh2^{-/-}$ brains, stained with the same anti-bodies, had normal levels of CCM2 and reduced levels of KRIT1. In stage 1 or stage 2 lesions from these four $Ccm1^{+/-}Msh2^{-/-}$ mice (Fig. 6), KRIT1 was either absent or reduced in the endothelial cells lining the caverns. Haploin-sufficiency of *Ccm1* would reduce, but not eliminate, KRIT1 expression in all cells expressing the transcript. However, loss of heterozygosity caused by a somatic mutation in a subset of endothelial cells would result in a null $Ccm1^{-/-}$ genotype, with the complete absence of KRIT1 protein expression in these cells alone, producing a mosaic expression pattern in the lesions. From these data, it is clear that in the lesions from $Ccm1^{+/-}Msh2^{-/-}$ animals, KRIT1 protein is not expressed in some of the endothelial cells lining the cavern. The mosaic nature of this loss of expression also suggests that a somatic mutation has occurred to inactivate the wild-type copy of *Ccm1* in a subset of these endothelial cells.

Ultrastructural changes in CCM lesions by electron microscopy

Electron micrographs from human CCM lesion samples have revealed large gaps in the endothelial cell layer and other
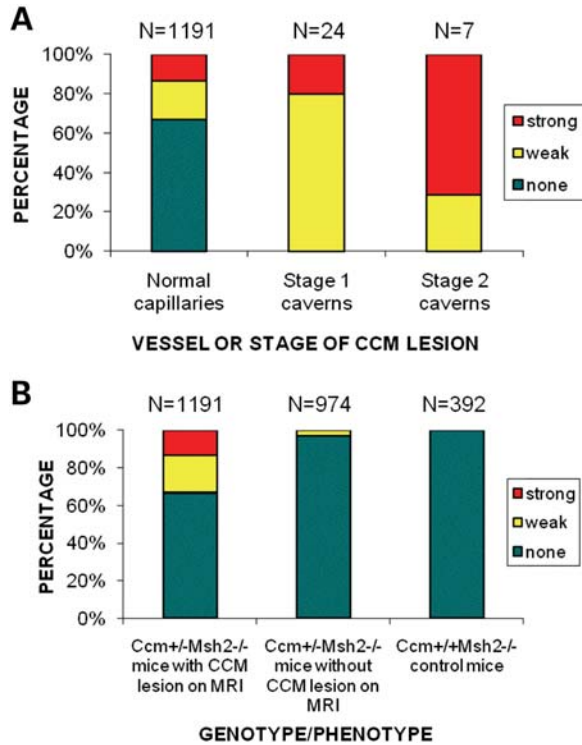
Figure 5. ROCK activation increases as CCM lesions grow. (**A**) The relative intensities of pMLC staining were compared between normal capillaries, stage 1 CCM lesions and stage 2 lesions. The intensity of pMLC staining increases with the size and complexity of the lesions in $Ccm1^{+/-}Msh2^{-/-}$ mouse brains with CCMs (regression coefficient = 0.7655, $P < 0.0001$; common odds ratio = 2.150). (**B**) The pMLC staining intensities of normal capillaries were compared between the genotypes and MRI phenotypes of the mice. Normal capillaries in brains from $Ccm1^{+/-}Msh2^{-/-}$ mice with CCM lesions show stronger pMLC staining than those from mice with the same genotype without CCM lesions, which in turn show stronger pMLC staining than those from $Msh2^{-/-}$ control mice ($P < 0.0001$, exact Mantel–Haenszel test). *Post hoc* Bonferroni-adjusted P-values were <0.001 between two groups in all three comparisons.

defects in blood-brain barrier ultrastructure (16–18). If the CCM lesions in this mouse model follow the same development and pathology as those in humans, we would expect to document similar pathology by electron microscopy. Transmission electron microscopy demonstrated capillary endothelial cells in wild-type C57BL/6 control mice with flat ovoid nuclei; all tight junctions between endothelial cells were intact, with surrounding pericytes, a defined basement membrane layer and astrocytic foot processes (Fig. 7). Normal capillaries in $Ccm1^{+/-}Msh2^{-/-}$ and $Ccm2^{+/-}Msh2^{-/-}$ mice had similar features, including grossly normal morphology of endothelial cells, tight junctions, pericytes and basement membrane. Several CCM lesions in $Ccm1^{+/-}Msh2^{-/-}$ mice included blood-filled caverns of different sizes. The shape of endothelial cells lining those caverns and their nuclei appeared the same as in control capillaries, but there were no typical pericytes or basement membrane surrounding the endothelial cell layer in CCM lesions. The majority of tight junctions between endothelial cells lining the caverns appeared morphologically normal. However, we observed filopodia in endothelial cells of the larger caverns and several gaps in endothelial cells, with

instances of grossly extravasated erythrocytes. These features resemble those previously reported for human CCM lesions (16–18), so this model allows us to begin to study more carefully the nature and extent of ultrastructural defects associated with lesions at various stages of development.

DISCUSSION

The two-hit mutational mechanism for CCM pathogenesis is supported by numerous clinical and molecular observations. Clinically, sporadic cases are characterized by solitary lesions, whereas autosomal dominant cases are characterized by multiple lesions (44). The two-hit mechanism is also supported by clinical observations of increasing lesion burden throughout the life in humans with heterozygous germline mutations (22,23). In further support of this hypothesis, biallelic somatic mutations have been recently found in surgically resected mature lesions from CCM patients (24–26). Despite these observations, the relationship of these somatic mutations to lesion genesis remains uncertain. An experimental model is needed to investigate this connection.

Like other mouse models of human inherited disease, the *Ccm1* and *Ccm2* heterozygous mutant mice do not faithfully recapitulate the CCM human disease phenotype. Autosomal dominant diseases that have been shown to follow a two-hit mutational mechanism are often difficult to model in mice. Mice have a much shorter lifespan than humans, and the number of relevant target cells is often much less, leading to a greatly reduced chance for a random, biallelic somatic mutation to occur during the lifetime of the animal. In such cases, moving the orthologous gene mutation into a different genetic background can often generate a more faithful animal model while also revealing important aspects of disease pathogenesis.

The *Msh2* gene is a critical component of the mismatch-repair complex, and the loss of this protein leads to an increased somatic mutation load (35,45–48). Using an *Msh2*-null sensitized background for the *Ccm1* heterozygous mice, we have created a mouse model of CCM that faithfully recapitulates the phenotype of mature CCM lesions, as well as lesions at earlier stages of development. These mice develop CCM lesions with a penetrance near 50%. The development of CCM lesions occurred specifically in $Ccm1^{+/-}Msh2^{-/-}$ mice. Neither unsensitized $Ccm1^{+/-}$ or $Ccm2^{+/-}$ mice, nor $Msh2^{-/-}$ controls develop CCM lesions, consistent with the $Msh2^{-/-}$ genotype acting as a sensitized genetic background rather than the primary cause of CCM lesion genesis. The stochastic nature of the murine CCM lesions in both penetrance and localization also replicate what is seen in humans. It is unlikely that the results of our model are confounded by the cancer predisposition *per se*, as vascular malformations have not been reported in humans with $MSH2^{-/-}$ germline mutations (Lynch Syndrome) (49). While cancer phenotypes are a concern in $Msh2^{-/-}$ mice, these mice rarely develop brain tumors, and animal attrition rates are favorably low in comparison to those with *Trp53*-null background (31,32). This new, more penetrant model enables the study of the natural history of lesions.
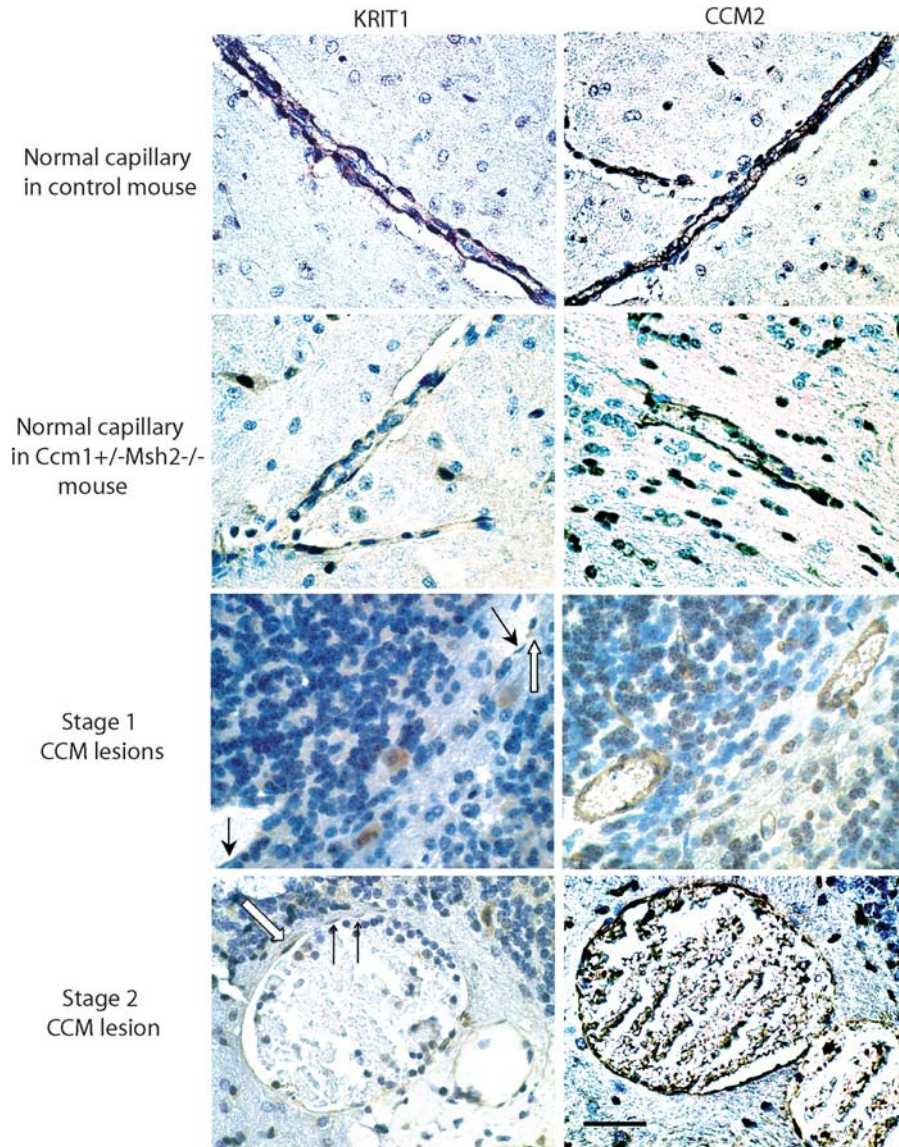
Figure 6. Reduced KRIT1 expression in the endothelium of mouse CCM lesions. Capillaries in $Msh2^{-/-}$ control brains (first row) showed prominent brown staining for both KRIT1 (left) and CCM2 (right). Consistent with the genotype of the mice, KRIT1 staining was reduced, while CCM2 staining remained at control levels in normal capillaries (second row) of the $Ccm1^{+/-}Msh2^{-/-}$ mouse brain. Endothelial cells lining two stage 1 CCM lesions (third row) and two caverns of a stage 2 CCM lesion (fourth row) showed normal staining for CCM2 (right), but either reduced (white arrow) or no staining (black arrow) for KRIT1 (left). Scale bar is 50 μm.

Unlike the $Ccm1^{+/-}Msh2^{-/-}$ mice that exhibit both early and late-stage CCM lesions, we did not observe cerebrovascular lesions in the 11 $Ccm2^{+/-}Msh2^{-/-}$ mice. In contrast, somatic mutations have been found in mature CCM lesions from patients harboring *CCM1*, *CCM2* or *CCM3* germline mutations (24–26), suggesting that all forms of inherited CCM follow a two-hit mutational mechanism. Since the murine *Ccm1* coding region (2211 nucleotides) is nearly twice the size of that of murine *Ccm2* (1362 nucleotides), the random, stochastic nature of somatic mutagenesis in the mismatch repair-deficient sensitized mice may favor lesion genesis in the *Ccm1* model harboring the larger target. However, this size difference alone would not be expected to account for the apparent lack of penetrance in the $Ccm2^{+/-}Msh2^{-/-}$ model. We do not

believe that this invalidates the two-hit hypothesis for *Ccm2* pathogenesis, as this mechanism is supported by the human somatic mutation data (25,27) and by our original CCM2 mouse model (32). We have previously observed cerebrovascular lesions with significant penetrance (33%) in both $Ccm1^{+/-}Trp53^{-/-}$ and $Ccm2^{+/-}Trp53^{-/-}$ mouse models of CCM (31,32). *Trp53* deficiency causes widespread somatic genomic instability including an increase in the frequency of deletions and other gross chromosomal changes (33). To date, we cannot explain why *Trp53* deficiency sensitizes the *Ccm2* heterozygous mice to develop CCM lesions while *Msh2* deficiency does not. This difference requires further study and may reflect key differences between CCM1 and CCM2 pathogenesis.
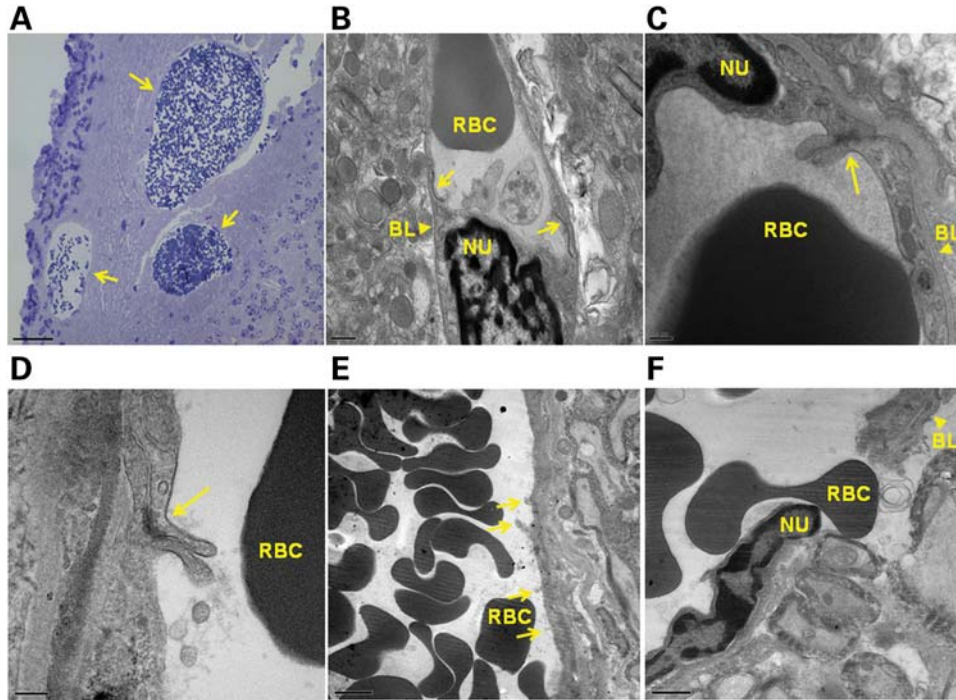
Figure 7. Electron microscopy reveals abnormal ultrastructure of CCM lesion endothelium. (**A**) Three CCM lesions (arrows) in a $Ccm1^{+/-}Msh2^{-/-}$ mouse brain shown by Toluidine Blue staining ($\times 40$, scale bar 25 μm). (**B**) Intact tight junctions (arrows) and basal lamina (arrowheads) are present within a normal capillary in a control C57BL/6 mouse ($\times 4600$, scale bar 1 μm). Intact tight junctions (arrows) and basal lamina (arrowheads) are also present within a normal capillary (**C**, $\times 35000$, scale bar 200 nm) and a CCM lesion (**D**, $\times 35000$, scale bar 200 nm) in a $Ccm1^{+/-}Msh2^{-/-}$ mouse brain. (**E**) In the same lesion, filopodia (arrows) are present ($\times 4060$, scale bar 2 μm). (**F**) A tight junction and the basal lamina (arrowhead) are both broken in this lesion and erythrocyte extravasation is visible ($\times 8260$, scale bar 1 μm). RBC, red blood cell; NU, endothelial nucleus; BL, basal lamina.

The $Ccm1^{+/-}Msh2^{-/-}$ mouse model provides additional evidence for a two-hit mechanism for CCM lesion genesis. Increasing genetic instability and the rate of somatic mutations by homozygous knockout of *Msh2* suggests that a somatic second mutation promotes CCM lesion development. We have made repeated attempts to identify somatic second mutations in the murine lesions, using the same approach as we used for human CCM lesions (25). Unfortunately, we have reached a technical limit with the analysis of the murine lesions. The murine lesions are comparatively much smaller than the human lesions, resulting in a paucity of cellular material for molecular analysis. With increased rounds of amplification to generate sufficient DNA for cloning and sequencing, distinguishing *bona fide* somatic mutations from polymerase chain reaction (PCR)-induced errors became a serious problem that is easily avoided with the larger human lesions. This remained true even when we obtained deep sequence coverage using next-generation DNA sequencing. With the deeper coverage, the signal-to-noise distinction became even more problematic.

In lieu of DNA sequence data, the KRIT1 immunohistochemistry data show a mosaic lack of staining in the murine lesions as direct evidence of loss of expression, which indirectly suggests that somatic mutation occurred (27). The mosaic absence of KRIT1 protein from stage 1 lesions of $Ccm1^{+/-}Msh2^{-/-}$ animals strongly suggest that lesion growth is initiated by the loss of functional CCM protein. While this evidence is indirect, it supports the two-hit hypothesis as the genetic mechanism of the initial stages of CCM lesion genesis.

From multiple lines of evidence, the murine lesions observed in this model appear identical to those seen in CCM patients. The integrity of the endothelial cell layer and other blood–brain barrier ultrastructure are often compromised in human CCM lesions, leaving gaps of almost a micron between endothelial cells (16–18). This has been proposed to be the etiology of the vascular leakage and hemorrhage associated with clinical symptoms of CCM disease. *In vitro* work has shown that while knockdown of KRIT1 by siRNA had no effect on tight junction protein expression, it did cause an increase in permeability of *in vitro* endothelial cell monolayers (11). Other *in vitro* and *in vivo* studies have supported an increase in permeability after loss of CCM expression (12,14). The electron microscopy data provide clear evidence that the CCM lesions in this mouse model manifest the same ultrastructural defects in blood–brain barrier as human lesions, including gross gaps in endothelial layer integrity, accounting for increased permeability. But these preliminary results demonstrate apparently normal tight junctions between most endothelial cells in cavern wall, consistent with normal *in vitro* tight junction protein expression.

This new model of CCM is the first means of studying the molecular mechanisms of lesion genesis and progression *in vivo*. Studies of early lesions have been limited in humans because typical MRI using gradient-echo or fast spin-echo

protocols can only detect the largest lesions. More recently, susceptibility-weighted imaging (SWI) has been used to identify much smaller lesions and potential pre-lesions in sharp detail (28). Based on our work with this new mouse model, it appears that the earliest lesions manifest far less iron deposit, cell proliferation and inflammatory infiltrate, yet they already manifest as grossly dilated capillaries with cavernous structure. For the first time, we have shown evidence that some late-stage human CCM lesion phenotypes are beginning to develop in the earlier stages of the lesion formation.

While late-stage CCM lesions from humans and mice show an increase in pMLC levels (14), an indicator of ROCK activity, a modest, but significant, increase in pMLC is observed in the early lesion. The pMLC expression was significantly stronger in normal capillaries of animals harboring CCM lesions than in animals of the same genotype without lesions. We speculate that animals may have a range of background ROCK activation due to a variety of factors, and those with inherently greater ROCK activation (background pMLC expression) are more likely to develop lesions. Recent studies have shown that ROCK inhibitors, such as fasudil and statins, can reverse some of the phenotypes associated with the loss of CCM proteins (12,14). These studies were performed in in vitro systems or in mice without CCM lesions, so the advent of this in vivo CCM mouse model provides an opportunity to investigate the effects of ROCK inhibitors on the development, growth and maturation of CCM lesions.

Using these mice, it will be possible to study how apparently normal vessels can, over time, develop into the large, multicavernous lesions that are the hallmark of CCM. We will also be able to test therapeutic interventions that may improve the quality of life of CCM patients. It is uncertain if a single treatment would be sufficient to fully treat CCM or if multiple pharmacologic agents may be necessary. For instance, inhibition of ROCK may be effective at early stages of disease development while anti-angiogenic, anti-proliferative or anti-inflammatory strategies may be more effective at later stages of lesion maturation. In the best-case scenario, we may find particular therapeutics that can reverse or prevent lesion growth. Since this CCM mouse model produces lesions at varying stages of development, we will be able to fully test the best therapeutic strategies that may be used in a clinical setting.

An alternative approach to CCM animal model development is the use of conditional knockout of the CCM genes to create an artificial, tissue-specific, homozygous state within a specific time window, averting embryonic lethality. A conditional knockout acutely induces inactivation of particular genes in an entire population of cells. By contrast, our sensitized model induces stochastic somatic mosaicism within a population of cells, which more closely resembles what has been observed in human lesions (25,27). When models based on conditional knockout alleles are available and characterized, it will be useful to compare their relative relevance to the human disease. In fact, both the *Msh2* sensitized model and the conditional knockout model could provide complementary information about mechanisms of the human disease. To date, our model is the first to report a wide range of phenotypic similarities to human CCM lesions.

MATERIALS AND METHODS

Mice

All animal procedures were approved by the Duke University Institutional Animal Care and Use Committee. Mice were genotyped by PCR for *Ccm1* (29), *Ccm2* (30), *Msh2* (39) and CRE recombinase (Jackson Laboratories protocol). Unless otherwise noted, upon sacrifice the brain of each mouse was carefully removed and immediately immersed in 10% formalin for fixation.

MRI protocol

MRI was conducted on formalin-fixed murine brains using either a 14.1 T (600 MHz) or a 9.4 T (400 MHz) Bruker Avance imaging spectrometer. Three-dimensional-gradient recalled echo (T_2*-weighted) images were acquired *ex vivo* as described previously (32).

Iron staining and immunohistochemistry

Chemical detection of iron deposits in mice with CCM lesions was performed by a Perls' Prussian stain method. Five millimeter-thick slices of mouse brain were treated by fresh solution of 20% hydrochloric acid and 10% potassium ferrocyanide and counterstained with nuclear fast red. Adjacent sections were stained by immunohistochemistry for macrophages, B cells, plasma cells and proliferation-associated nuclear protein Ki-67. The sections were treated for antigen retrieval using DAKO buffer (pH 6.0). Endogenous peroxidase was extinguished with 3% hydrogen peroxide. Staining was performed with the avidin–biotin complex technique using the Vectastain ABC kit (Vector Laboratories, Burlingame, CA, USA). The primary antibodies used were mouse monoclonal anti-CD11b (macrophages) antibody (eBioscience, rat IgG, 14-0112-81, 1:500), mouse monoclonal anti-B220 (B-cells) antibody (BD Biosciences, rat IgG, 550286, 1:500), mouse monoclonal anti-CD138 (plasma cells) antibody (BD Biosciences, rat IgG, 553712, 1:500) or mouse monoclonal anti-Ki67 antibody (DAKO, rat IgG, clone TEC-3, M7249, 1:75). A biotinylated rabbit anti-rat secondary antibody (Vector Lab, BA 4000 rabbit anti-rat IgG biotinylated, 1:50) was then administered. Negative controls were performed throughout the entire immunohistochemistry procedure.

Paraffin-embedded 5 μm tissue sections of mouse cerebral lesion specimens were deparaffinized by serial washing in first xylenes and then ethanol dilutions (100, 95 and 70%). Endogenous peroxidase was neutralized by 3% H_2O_2 in methanol for 30 min. Antigen retrieval was performed using citrate-buffered antigen retrieval solution (Vector Laboratories). Sections were blocked using PBS–FSGO [phosphate-buffered saline supplemented with 0.5% fish skin gelatin (FSGO), Sigma-Aldrich, St Louis, MO, USA] and 5% goat serum (Invitrogen, Carlsbad, CA, USA) and then biotin-blocked (Vector Laboratories). Slides were probed with anti-KRIT1 6832 (Ginsberg Lab, UCSD; 1 mg/ml affinity purified rabbit polyclonal antibody, immunogen GST-tagged recombinant protein corresponding to human KRIT1 FERM domain) at 1:250 in PBS–FSGO; rabbit polyclonal anti-CCM2 (Abnova, Taipei City, Taiwan; immunogen corresponds to

full-length human CCM protein) at 1:250, or rabbit polyclonal anti-pMLC [Thr^{180}/Ser^{19}] (Cell Signaling Technology, MA, USA) at 1:250, as previously described ([14](14)); control sections were treated with 1.5 µg/ml of rabbit IgG (Santa Cruz Biotechnology, Inc., Santa Cruz, CA, USA). All primary antibody incubations were performed overnight at 4°C, covered, in a humidified chamber. Slides were then washed and probed with biotinylated goat anti–rabbit IgG (1:1000, Vector Laboratories) overnight at 4°C in a humidified chamber, washed in PBS–FSGO and incubated with Elite ABC kit reagents (Vector Laboratories) for 30 min at room temperature. Color was developed using DAB substrate (3,3′-diaminobenzidine) for 5 min. Slides were washed and counterstained with Hematoxylin QS (Vector Laboratories) for 1 min, washed and sequentially dehydrated with absolute ethanol, then xylenes, mounted with Vectashield, and photographed using a brightfield microscope (Leica, Bannockburn, IL, USA) with digital camera (Diagnostic Instruments, Sterling Heights, MI, USA).

pMLC staining was assessed as 'none' (completely absent stain), 'weak' (definite, but diffuse) and 'strong' (intense and confluent) independently by two investigators (R.S. and C.S.). In order to analyze the pMLC staining data, a Poisson distribution was assumed to construct an ordinal log linear model and a log link function. The significance of a linear-by-linear association was assessed by the Chi-square test using SAS 9.2 PROC GENMOD.

Transmission electron microscopy

Brains were carefully removed from the mice and immediately immersed in freshly prepared 4% paraformaldehyde. After 24 h, the brain was sliced into 1 mm thick coronal sections and observed for possible lesions under a dissecting microscope. Regions that contain suspected lesions were cut into 1 mm cubes and placed into PBS at 4°C. Specimens were post-fixed with 1% osmium tetroxide, dehydrated in a graded series of ethanol and embedded in epoxy resin. Representative areas of interest were identified by light microscopy-stained Toluidine Blue staining. Sections were stained with uranyl acetate and lead citrate, viewed on a Philips CM 10 transmission electron microscope and images were captured using a Gatan ES1000W digital camera. Morphological changes were detected in a blinded fashion by two investigators.

REFERENCES

1. Del Curling, O. Jr, Kelly, D.L. Jr, Elster, A.D. and Craven, T.E. (1991) An analysis of the natural history of cavernous angiomas. *J. Neurosurg.*, **75**, 702–708.
2. Otten, P., Pizzolato, G.P., Rilliet, B. and Berney, J. (1989) 131 cases of cavernous angioma (cavernomas) of the CNS, discovered by retrospective analysis of 24,535 autopsies. *Neurochirurgie*, **35**, 82–83.
3. Laberge-le Couteulx, S., Jung, H.H., Labauge, P., Houtteville, J.P., Lescoat, C., Cecillon, M., Marechal, E., Joutel, A., Bach, J.F. and Tournier-Lasserve, E. (1999) Truncating mutations in CCM1, encoding KRIT1, cause hereditary cavernous angiomas. *Nat. Genet.*, **23**, 189–193.
4. Sahoo, T., Johnson, E.W., Thomas, J.W., Kuehl, P.M., Jones, T.L., Dokken, C.G., Touchman, J.W., Gallione, C.J., Lee-Lin, S.Q., Kosofsky, B. *et al.* (1999) Mutations in the gene encoding KRIT1, a Krev-1/rap1a binding protein, cause cerebral cavernous malformations (CCM1). *Hum. Mol. Genet.*, **8**, 2325–2333.
5. Liquori, C.L., Berg, M.J., Siegel, A.M., Huang, E., Zawistowski, J.S., Stoffer, T., Verlaan, D., Balogun, F., Hughes, L., Leedom, T.P. *et al.* (2003) Mutations in a gene encoding a novel protein containing a phosphotyrosine-binding domain cause type 2 cerebral cavernous malformations. *Am. J. Hum. Genet.*, **73**, 1459–1464.
6. Denier, C., Goutagny, S., Labauge, P., Krivosic, V., Arnoult, M., Cousin, A., Benabid, A.L., Comoy, J., Frerebeau, P., Gilbert, B. *et al.* (2004) Mutations within the MGC4607 gene cause cerebral cavernous malformations. *Am. J. Hum. Genet.*, **74**, 326–337.
7. Bergametti, F., Denier, C., Labauge, P., Arnoult, M., Boetto, S., Clanet, M., Coubes, P., Echenne, B., Ibrahim, R., Irthum, B. *et al.* (2005) Mutations within the programmed cell death 10 gene cause cerebral cavernous malformations. *Am. J. Hum. Genet.*, **76**, 42–51.
8. Zawistowski, J.S., Stalheim, L., Uhlik, M.T., Abell, A.N., Ancrile, B.B., Johnson, G.L. and Marchuk, D.A. (2005) CCM1 and CCM2 protein interactions in cell signaling: implications for cerebral cavernous malformations pathogenesis. *Hum. Mol. Genet.*, **14**, 2521–2531.
9. Goudreault, M., D'Ambrosio, L.M., Kean, M.J., Mullin, M.J., Larsen, B.G., Sanchez, A., Chaudhry, S., Chen, G.I., Sicheri, F., Nesvizhskii, A.I. *et al.* (2009) A PP2A phosphatase high density interaction network identifies a novel striatin-interacting phosphatase and kinase complex linked to the cerebral cavernous malformation 3 (CCM3) protein. *Mol. Cell Proteomics*, **8**, 157–171.
10. Hilder, T.L., Malone, M.H., Bencharit, S., Colicelli, J., Haystead, T.A., Johnson, G.L. and Wu, C.C. (2007) Proteomic identification of the cerebral cavernous malformation signaling complex. *J. Proteome Res.*, **6**, 13.
11. Glading, A., Han, J., Stockton, R.A. and Ginsberg, M.H. (2007) KRIT-1/CCM1 is a Rap1 effector that regulates endothelial cell cell junctions. *J. Cell Biol.*, **179**, 247–254.
12. Whitehead, K.J., Chan, A.C., Navankasattusas, S., Koh, W., London, N.R., Ling, J., Mayo, A.H., Drakos, S.G., Marchuk, D.A., Davis, G.E. *et al.* (2009) The cerebral cavernous malformation signaling pathway promotes vascular integrity via Rho GTPases. *Nat. Med.*, **15**, 177–184.
13. Borikova, A.L., Dibble, C.F., Sciaky, N., Welch, C.M., Abell, A.N., Bencharit, S. and Johnson, G.L. (2010) Rho kinase inhibition rescues the endothelial cell cerebral cavernous malformation phenotype. *J. Biol. Chem.*, **285**, 11760–11764.
14. Stockton, R.A., Shenkar, R., Awad, I.A. and Ginsberg, M.H. (2010) Cerebral cavernous malformations proteins inhibit Rho kinase to stabilize vascular integrity. *J. Exp. Med.*, **207**, 881–896.
15. Crose, L.E., Hilder, T.L., Sciaky, N. and Johnson, G.L. (2009) Cerebral cavernous malformation 2 protein promotes smad ubiquitin regulatory factor 1-mediated RhoA degradation in endothelial cells. *J. Biol. Chem.*, **284**, 13301–13305.
16. Wong, J.H., Awad, I.A. and Kim, J.H. (2000) Ultrastructural pathological features of cerebrovascular malformations: a preliminary report. *Neurosurgery*, **46**, 1454–1459.
17. Clatterbuck, R.E., Eberhart, C.G., Crain, B.J. and Rigamonti, D. (2001) Ultrastructural and immunocytochemical evidence that an incompetent blood-brain barrier is related to the pathophysiology of cavernous malformations. *J. Neurol. Neurosurg. Psychiatry*, **71**, 188–192.
18. Tu, J., Stoodley, M.A., Morgan, M.K. and Storer, K.P. (2005) Ultrastructural characteristics of hemorrhagic, nonhemorrhagic, and recurrent cavernous malformations. *J. Neurosurg.*, **103**, 903–909.

19. Shenkar, R., Elliott, J.P., Diener, K., Gault, J., Hu, L.J., Cohrs, R.J., Phang, T., Hunter, L., Breeze, R.E. and Awad, I.A. (2003) Differential gene expression in human cerebrovascular malformations. *Neurosurgery*, **52**, 465–477; discussion 477–468.

20. Shi, C., Shenkar, R., Du, H., Duckworth, E., Raja, H., Batjer, H.H. and Awad, I.A. (2009) Immune response in human cerebral cavernous malformations. *Stroke*, **40**, 1659–1665.

21. Shi, C., Shenkar, R., Batjer, H.H., Check, I.J. and Awad, I.A. (2007) Oligoclonal immune response in cerebral cavernous malformations. Laboratory investigation. *J. Neurosurg.*, **107**, 1023–1026.

22. Labauge, P., Brunereau, L., Levy, C., Laberge, S. and Houtteville, J.P. (2000) The natural history of familial cerebral cavernomas: a retrospective MRI study of 40 patients. *Neuroradiology*, **42**, 327–332.

23. de Champfleur, N.M., Langlois, C., Ankenbrandt, W.J., Le Bars, E., Leroy, M.A., Duffau, H., Bonafe, A., Jaffe, J., Awad, I.A. and Labauge, P. (2010) MRI evalution of cerebral cavernous maflormations with susceptibility-weighted imaging. *Neurosurgery*, in press.

24. Gault, J., Shenkar, R., Recksiek, P. and Awad, I.A. (2005) Biallelic somatic and germ line CCM1 truncating mutations in a cerebral cavernous malformation lesion. *Stroke*, **36**, 872–874.

25. Akers, A.L., Johnson, E., Steinberg, G.K., Zabramski, J.M. and Marchuk, D.A. (2009) Biallelic somatic and germline mutations in cerebral cavernous malformations (CCMs): evidence for a two-hit mechanism of CCM pathogenesis. *Hum. Mol. Genet.*, **18**, 919–930.

26. Gault, J., Awad, I.A., Recksiek, P., Shenkar, R., Breeze, R., Handler, M. and Kleinschmidt-DeMasters, B.K. (2009) Cerebral cavernous malformations: somatic mutations in vascular endothelial cells. *Neurosurgery*, **65**, 138–144; discussion 144–135.

27. Pagenstecher, A., Stahl, S., Sure, U. and Felbor, U. (2009) A two-hit mechanism causes cerebral cavernous malformations: complete inactivation of CCM1, CCM2 or CCM3 in affected endothelial cells. *Hum. Mol. Genet.*, **18**, 911–918.

28. de Souza, J.M., Domingues, R.C., Cruz, L.C. Jr, Domingues, F.S., Iasbeck, T. and Gasparetto, E.L. (2008) Susceptibility-weighted imaging for the evaluation of patients with familial cerebral cavernous malformations: a comparison with t2-weighted fast spin-echo and gradient-echo sequences. AJNR. *Am. J. Neuroradiol.*, **29**, 154–158.

29. Whitehead, K.J., Plummer, N.W., Adams, J.A., Marchuk, D.A. and Li, D.Y. (2004) Ccm1 is required for arterial morphogenesis: implications for the etiology of human cavernous malformations. *Development*, **131**, 1437–1448.

30. Plummer, N.W., Squire, T.L., Srinivasan, S., Huang, E., Zawistowski, J.S., Matsunami, H., Hale, L.P. and Marchuk, D.A. (2006) Neuronal expression of the Ccm2 gene in a new mouse model of cerebral cavernous malformations. *Mamm. Genome*, **17**, 119–128.

31. Plummer, N.W., Gallione, C.J., Srinivasan, S., Zawistowski, J.S., Louis, D.N. and Marchuk, D.A. (2004) Loss of p53 sensitizes mice with a mutation in Ccm1 (KRIT1) to development of cerebral vascular malformations. *Am. J. Pathol.*, **165**, 1509–1518.

32. Shenkar, R., Venkatasubramanian, P.N., Wyrwicz, A.M., Zhao, J.C., Shi, C., Akers, A., Marchuk, D.A. and Awad, I.A. (2008) Advanced magnetic resonance imaging of cerebral cavernous malformations: part II. Imaging of lesions in murine models. *Neurosurgery*, **63**, 790–797; discussion 797–798.

33. Shao, C., Deng, L., Henegariu, O., Liang, L., Stambrook, P.J. and Tischfield, J.A. (2000) Chromosome instability contributes to loss of heterozygosity in mice lacking p53. *Proc. Natl Acad. Sci. USA*, **97**, 7405–7410.

34. Donehower, L.A., Harvey, M., Slagle, B.L., McArthur, M.J., Montgomery, C.A. Jr, Butel, J.S. and Bradley, A. (1992) Mice deficient for p53 are developmentally normal but susceptible to spontaneous tumours. *Nature*, **356**, 215–221.

35. Hegan, D.C., Narayanan, L., Jirik, F.R., Edelmann, W., Liskay, R.M. and Glazer, P.M. (2006) Differing patterns of genetic instability in mice deficient in the mismatch repair genes Pms2, Mlh1, Msh2, Msh3 and Msh6. *Carcinogenesis*, **27**, 2402–2408.

36. Reitmair, A.H., Cai, J.C., Bjerknes, M., Redston, M., Cheng, H., Pind, M.T., Hay, K., Mitri, A., Bapat, B.V., Mak, T.W. *et al.* (1996) MSH2 deficiency contributes to accelerated APC-mediated intestinal tumorigenesis. *Cancer Res.*, **56**, 2922–2926.

37. Song, J., Sohn, K.J., Medline, A., Ash, C., Gallinger, S. and Kim, Y.I. (2000) Chemopreventive effects of dietary folate on intestinal polyps in Apc+/−Msh2−/− mice. *Cancer Res.*, **60**, 3191–3199.

38. Lal, G., Ash, C., Hay, K., Redston, M., Kwong, E., Hancock, B., Mak, T., Kargman, S., Evans, J.F. and Gallinger, S. (2001) Suppression of intestinal polyps in Msh2-deficient and non-Msh2-deficient multiple intestinal neoplasia mice by a specific cyclooxygenase-2 inhibitor and by a dual cyclooxygenase-1/2 inhibitor. *Cancer Res.*, **61**, 6131–6136.

39. Kucherlapati, M.H., Lee, K., Nguyen, A.A., Clark, A.B., Hou, H. Jr, Rosulek, A., Li, H., Yang, K., Fan, K., Lipkin, M. *et al.* (2010) An Msh2 conditional knockout mouse for studying intestinal cancer and testing anticancer agents. *Gastroenterology*, **138**, 880–882.

40. de Wind, N., Dekker, M., Berns, A., Radman, M. and te Riele, H. (1995) Inactivation of the mouse Msh2 gene results in mismatch repair deficiency, methylation tolerance, hyperrecombination, and predisposition to cancer. *Cell*, **82**, 321–330.

41. Reitmair, A.H., Schmits, R., Ewel, A., Bapat, B., Redston, M., Mitri, A., Waterhouse, P., Mittrucker, H.W., Wakeham, A., Liu, B. *et al.* (1995) MSH2 deficient mice are viable and susceptible to lymphoid tumours. *Nat. Genet.*, **11**, 64–70.

42. Sure, U., Butz, N., Schlegel, J., Siegel, A.M., Wakat, J.P., Mennel, H.D., Bien, S. and Bertalanffy, H. (2001) Endothelial proliferation, neoangiogenesis, and potential de novo generation of cerebrovascular malformations. *J. Neurosurg.*, **94**, 972–977.

43. Shenkar, R., Sarin, H., Awadallah, N.A., Gault, J., Kleinschmidt-DeMasters, B.K. and Awad, I.A. (2005) Variations in structural protein expression and endothelial cell proliferation in relation to clinical manifestations of cerebral cavernous malformations. *Neurosurgery*, **56**, 343–354.

44. Rigamonti, D., Hadley, M.N., Drayer, B.P., Johnson, P.C., Hoenig-Rigamonti, K., Knight, J.T. and Spetzler, R.F. (1988) Cerebral cavernous malformations. Incidence and familial occurrence. *N. Engl. J. Med.*, **319**, 343–347.

45. Modrich, P. and Lahue, R. (1996) Mismatch repair in replication fidelity, genetic recombination, and cancer biology. *Annu. Rev. Biochem.*, **65**, 101–133.

46. Burr, K.L., van Duyn-Goedhart, A., Hickenbotham, P., Monger, K., van Buul, P.P. and Dubrova, Y.E. (2007) The effects of MSH2 deficiency on spontaneous and radiation-induced mutation rates in the mouse germline. *Mutat. Res.*, **617**, 147–151.

47. Campbell, M.R., Wang, Y., Andrew, S.E. and Liu, Y. (2006) Msh2 deficiency leads to chromosomal abnormalities, centrosome amplification, and telomere capping defect. *Oncogene*, **25**, 2531–2536.

48. Baross-Francis, A., Andrew, S.E., Penney, J.E. and Jirik, F.R. (1998) Tumors of DNA mismatch repair-deficient hosts exhibit dramatic increases in genomic instability. *Proc. Natl Acad. Sci. USA*, **95**, 8739–8743.

49. Jarvinen, H.J., Renkonen-Sinisalo, L., Aktan-Collan, K., Peltomaki, P., Aaltonen, L.A. and Mecklin, J.P. (2009) Ten years after mutation testing for Lynch syndrome: cancer incidence and outcome in mutation-positive and mutation-negative family members. *J. Clin. Oncol.*, **27**, 4793–4797.